Journal of Magnetic Resonance 248 (2014) 153–163

Contents lists available at ScienceDirect

Journal of Magnetic Resonance

journal homepage: www.elsevier.com/locate/jmr

Exploring diffusion across permeable barriers at high gradients. I. Narrow pulse approximation

Denis S. Grebenkov [a,*], Dang Van Nguyen [b], Jing-Rebecca Li [b,c]

[a] Laboratoire de Physique de la Matière Condensée, CNRS – Ecole Polytechnique, F-91128 Palaiseau, France
[b] CMAP, Ecole Polytechnique, F-91128 Palaiseau, France
[c] Neurospin, CEA Saclay, F-91191 Gif sur Yvette, France

ARTICLE INFO

Article history:
Received 11 April 2014
Revised 14 July 2014
Available online 15 August 2014

Keywords:
Bloch–Torrey equation
Permeability
Diffusion
Exchange

ABSTRACT

The adaptive variation of the gradient intensity with the diffusion time at a constant optimal *b*-value is proposed to enhance the contribution of the nuclei diffusing across permeable barriers, to the pulsed-gradient spin-echo (PGSE) signal. An exact simple formula the PGSE signal is derived under the narrow pulse approximation in the case of one-dimensional diffusion across a single permeable barrier. The barrier contribution to the signal is shown to be maximal at a particular *b*-value. The exact formula is then extended to multiple permeable barriers, while the PGSE signal is shown to be sensitive to the permeability and to the inter-barrier distance. Potential applications of the protocol to survey diffusion in three-dimensional domains with permeable membranes are illustrated through numerical simulations.

1. Introduction

Diffusion magnetic resonance imaging (dMRI) accesses geometrical, physiological, and functional properties of mineral porous media and biological tissues [1–9]. In most biological tissues, water exchange between compartments (e.g., cells and the extracellular space) plays an important role [10] while the permeability of cellular membranes may provide valuable physiological information (e.g., reduction of membrane permeability in stroke [11]).

Numerous works on water exchange and permeability estimation can be roughly split in three groups according to the underlying geometrical assumptions: (i) compartments of simple shapes (e.g., exchange between a sphere and the outer space, or between regularly spaced parallel barriers), (ii) effective compartments, and (iii) disordered media.

Brownstein and Tarr considered the signal attenuation in a spherical cellular compartment due to bulk and surface relaxations [12]. The surface relaxation modeled "leakage" of water molecules from the cellular compartment, under the simplifying assumption that the leaked molecules never return into the compartment. The solution of the governing diffusion equation was written in the form of a multi-exponential spectral decomposition over the Laplacian eigenfunctions, in which the multiple decay rates (Laplacian eigenvalues) were related to the permeability. In the fast-diffusion regime (or long time limit), the lowest eigenmode dominates, while the characteristic time is inversely proportional to the surface relaxivity (or permeability) [12]. This approach was further extended by Barzykin et al. who considered an exchange through the spherical boundary with the extracellular space [13]. In a first approximation, the presence of relaxing agents in the extracellular space was modeled by a partially absorbing boundary condition. Another, more accurate model of diffusion through a spherical interface into a rapidly relaxing extracellular space was then introduced and solved [14].

Tanner introduced a one-dimensional model of planar permeable barriers and calculated the apparent diffusion coefficient (ADC) that one would obtain from the pulsed-gradient spin-echo (PGSE) signal with very narrow gradient pulses [15]. In the long-time limit, the ADC is reduced to

$$D_{\rm eff} = D\left(1 + \frac{D}{\kappa \ell_b}\right)^{-1},$$

where D is the intrinsic (free) diffusion coefficient, κ the (diffusive) permeability, and ℓ_b the inter-barrier distance (see also [16]). Tanner used this model to estimate intercellular diffusion coefficients and membrane permeabilities for human red blood cells, adipose tissue, and brine shrimp [17] (see also [18]). Szafer et al. extended this approach to a two-dimensional model of parallel fibers of square cross-section [19], while Ford and Hackney applied it to calculate ADC in spinal cord injury and to estimate the permeability [20]. Several numerical schemes for computing PGSE signals in the

* Corresponding author.
E-mail address: denis.grebenkov@polytechnique.edu (D.S. Grebenkov).

http://dx.doi.org/10.1016/j.jmr.2014.07.013
1090-7807/

one-dimensional model of planar barriers have been reported [21–23]. Moreover, a matrix formalism was developed for rapid computation of PGSE signals in general multilayered structures with permeable membranes (e.g., arbitrary arrangement of parallel planes, co-axial cylinders or concentric spherical shells) [24]. An exact solution of the one-dimensional model with periodic permeable barriers was derived by Sukstanskii et al. [25] (see Section 2.7).

The second group of studies was initiated by Kärger and co-workers who introduced two co-existing pools of water molecules that both occupy the same volume of a voxel [26,27]. The exchange between pools was assumed to be uncorrelated from diffusion and to follow the standard linear kinetics (i.e., Poisson process). The assumption of isotropic Gaussian diffusion in each pool led to an explicit representation of the PGSE signal under the narrow pulse approximation (NPA), from which the residence times and volume fractions of water molecules in two pools can be estimated (the residence times being inversely proportional to the permeability). Although the explicit form of the PGSE signal made the Kärger model so attractive, naive identifications of the extracted volume fractions of two pools as volume fractions of the physiological constituents of the tissue, i.e., the cells (slow diffusion) and the extracellular space (fast diffusion), have failed [28–36]. Fieremans et al. proposed a coarse graining argument to justify the concept of two co-existing pools of water molecules, and validated the Kärger model by Monte Carlo simulations [37]. In particular, the slow exchange between compartments was shown to be necessary for two-compartment separation. For more permeable membranes, the exchange becomes correlated with diffusion, and the Kärger model tends to overestimate exchange times and thus to underestimate the permeability. The applicability conditions of the Kärger model are in favor for small cells with low permeability while its predictions for large cells (such as neuronal cell bodies) are less reliable. Coatleven et al. extended the Kärger model beyond the NPA and rigorously justified this extension by periodic homogenization technique [38]. The Kärger model has been modified in various ways to produce a more accurate approximation of the PGSE signal. Stanisz et al. extended the Kärger model to describe restricted diffusion in bovine optic nerve, in which prolate ellipsoids (axons) and spheres (glial cells) were surrounded by partially permeable membranes [39]. Similar approach with cylinders was developed by Meier et al. [40,41]. The Kärger model has been extensively applied to describe dMRI experiments in a variety of biological systems, e.g., suspension of erythrocytes [42–45], human breast cancer cells [46], yeast cells [34,47], and brain tissue [34,39–41,48–50]. Note that the underlying two-site exchange model was originally proposed by McConnell to account for kinetic molecular switches between two states [51] and then applied by many authors to estimate the cell permeability [45,52–56].

In the third group, one can mention the asymptotic approach developed by Mitra et al. who investigated the short-time behavior of the PGSE signal and showed the possibility to extract the surface-to-volume ratio, as well as permeability or surface relaxivity of general porous media [57–61]. Latour et al. measured the time-dependent diffusion coefficient in packed erythrocytes to estimate the erythrocyte membrane permeability and the surface-to-volume ratio of the cells [62].

Novikov et al. studied the effect of spatial configurations of permeable membranes onto the time-dependent diffusion coefficient [63,64] (see also [65]). They considered Brownian motion restricted by randomly placed and randomly oriented membranes. Using a scattering approach and the renormalization group solution, they related the long-time scaling behavior of the time-dependent diffusion coefficient to the strong structural fluctuations introduced by permeable membranes. While most earlier works assumed either compartments of simple shapes (spheres, cylinders, regularly spaced barriers, etc.) or shapeless compartments (Kärger's approach), the renormalization group technique was adequate for obtaining results for disordered media that resemble biological samples. The effect of permeability onto PGSE signals has also been studied through numerical simulations [36,66–68] (see also a review [69] on permeability influence on contrast enhancement).

The water permeability κ was determined experimentally and shown to vary significantly among biological tissues: 10^{-8} m/s for *Fundulus* eggs [70], $2\cdot 10^{-7}$ m/s for *Amoeba proteus* [71], $1.2\cdot 10^{-6}$ m/s for yeast cells [72], $2.7\cdot 10^{-6}$ m/s for the *Xenopus* oocyte [73], 10^{-5} m/s for axonal membranes and myelin sheath [28,74], $1.8\cdot 10^{-5}$ m/s for rat hepatocytes [75], $2.1\cdot 10^{-5}$ m/s for the *Chlorella* membrane [76], $3\cdot 10^{-5}$ m/s for acinar cell membranes [77], $(3-5)\cdot 10^{-5}$ m/s for human blood cell membranes [43,45], $7.4\cdot 10^{-5}$ m/s for the rat brain [78], $7.5\cdot 10^{-5}$ m/s for rabbit lung cells [79] (see also Refs. [49,80,81] that provide permeabilities for some other animal and plant cells). In order to reveal the role of permeability on PGSE signals, we will consider a broad range of permeabilities, from 10^{-6} m/s to 10^{-4} m/s.

In this paper, we propose a theoretical approach to explore diffusion across permeable barriers at high gradients under the narrow pulse approximation when diffusion during short gradient pulses can be ignored. Under this simplifying assumption, the PGSE signal is related to a pure diffusion propagator. We start by considering one-dimensional diffusion over a line with a single permeable barrier. For this problem the known diffusion propagator allows us to derive the exact explicit formula for the PGSE signal which is composed of two terms: the classical contribution from unrestricted diffusion, and the barrier contribution. We show that the barrier signal containing information on the permeability, exhibits a maximum at a certain gradient g_c which is inversely proportional to the diffusion length $\sqrt{D\Delta}$ (Δ being the diffusion time between gradient pulses). In other words, acquiring the signal at different diffusion times Δ and appropriately modified gradients allows one to maximize the contribution from the barrier. At zero permeability ($\kappa = 0$), the signal is simply a linear function of the diffusion length $\sqrt{D\Delta}$, while the water exchange at $\kappa > 0$ progressively reduces this dependence. At the next step, we apply these results to one-dimensional configurations of multiple permeable barriers. If the inter-barrier distance is much longer than $\sqrt{D\Delta}$, the barriers can be treated separately, and the above analysis provides, in addition, an estimate of the average inter-barrier distance. Moreover, varying the diffusion length $\sqrt{D\Delta}$, one can analyze mixed barrier configurations with small and large inter-barrier distances. Finally, we illustrate the potential use of this protocol on spherical and cubic cells, although its application to generic two- and three-dimensional systems with permeable membranes requires further investigations. In a forthcoming paper [82], we will remove the narrow pulse assumption and show how the signal at high gradients reveals diffusion across permeable barriers in the so-called localization regime.

2. Theoretical analysis

2.1. Diffusion propagator

The diffusive motion of the nuclei can be described by the diffusion propagator $G(x,y;t)$, i.e., the probability density for finding a nucleus started from y in a vicinity of x after time t. The diffusion propagator satisfies the diffusion equation

$$\frac{\partial}{\partial t}G(x,y;t) = D\frac{\partial^2}{\partial x^2}G(x,y;t), \tag{1}$$

with the initial condition

$$G(x,y;t=0) = \delta(x-y), \tag{2}$$

where $\delta(x)$ is the Dirac distribution. For unrestricted diffusion, the diffusion propagator takes the classical Gaussian form:

$$G_0(x,y;t) = \frac{1}{\sqrt{4\pi D t}} \exp\left(-\frac{(x-y)^2}{4Dt}\right). \quad (3)$$

Note that in the three-dimensional space, the second-order derivative $\partial^2/\partial x^2$ in Eq. (1) is replaced by the Laplace operator [3,83].

In the presence of obstacles or barriers, Eq. (1) has to be completed by interface or boundary conditions. We first consider the whole line with a single semi-permeable barrier at $x = 0$ that separates the positive and negative semi-axes. Two boundary conditions represent the flux conservation across the barrier, and the drop of magnetization due to permeation through the barrier:

$$\lim_{\epsilon\to 0}\left(D\frac{\partial}{\partial x}G(x,y;t)\right)_{x=+\epsilon} = \lim_{\epsilon\to 0}\left(D\frac{\partial}{\partial x}G(x,y;t)\right)_{x=-\epsilon} = \kappa\left[\lim_{\epsilon\to 0}G(-\epsilon,y;t) - \lim_{\epsilon\to 0}G(+\epsilon,y;t)\right], \quad (4)$$

where the approaches to the barrier at $x = 0$ from the negative axis and from the positive axis are distinguished explicitly. Here the same diffusion coefficient D is taken on the positive and negative semi-axes (one can also derive explicit results for the general case with two different diffusion coefficients). The limiting case $\kappa = 0$ describes two isolated compartments (with zero diffusive flux at $x = 0$). In the opposite limit of infinitely permeable barrier, $\kappa = \infty$ implies the continuity of the propagator $G(x,y;t)$ across the barrier: $\lim_{\epsilon\to 0}G(-\epsilon,y;t) = \lim_{\epsilon\to 0}G(+\epsilon,y;t)$. In intermediate cases ($0 < \kappa < \infty$), the propagator exhibits a discontinuity at the barrier due to its "resistance" to exchange.

The diffusion propagator satisfying Eqs. (1), (2), and (4) is

$$G(x,y;t) = \frac{\exp\left(-\frac{(x-y)^2}{4Dt}\right) + \exp\left(-\frac{(x+y)^2}{4Dt}\right)}{\sqrt{4\pi Dt}} - \frac{\kappa}{D}\exp\left(\frac{2\kappa}{D}(y+x+2\kappa t)\right)\operatorname{erfc}\left(\frac{y+x+4\kappa t}{2\sqrt{Dt}}\right),$$
$$G(x,y;t) = \frac{\kappa}{D}\exp\left(\frac{2\kappa}{D}(y-x+2\kappa t)\right)\operatorname{erfc}\left(\frac{y-x+4\kappa t}{2\sqrt{Dt}}\right), \quad (5)$$

where $\operatorname{erfc}(z)$ is the complementary error function, and the first (resp., second) relation corresponds to $x > 0$ (resp. $x < 0$). These expressions are valid for $y > 0$, while their extension to $y < 0$ is straightforward by relation $G(-x,-y;t) = G(x,y;t)$.

2.2. One-barrier signal

In a standard dMRI experiment, a 90° rf pulse flips the magnetization into the transverse plane, while two gradient pulses encode the diffusive motion of the nuclei [1,2]. When the duration of gradient pulses is (infinitely) short, diffusion *during* these pulses can be ignored so that the PGSE signal is related to the diffusion propagator [84,85]:

$$S = \int_{-\infty}^{\infty} dy\rho(y)\int_{-\infty}^{\infty} dx e^{iq(x-y)}G(x,y;\Delta), \quad (6)$$

where Δ is the diffusion time between two gradient pulses, $\rho(y)$ is the initial magnetization resulting from the 90° rf pulse excitation, and $q = \gamma g\delta$ is the wave vector[1] that incorporates the gyromagnetic ratio γ (e.g., $\gamma = 2.675\cdot 10^8$ rad/s/Tesla for water protons) and the strength g and duration δ of gradient pulses. Measuring the PGSE signal as a function of the gradient strength g, one aims at inferring diffusive properties of the medium through the averaged diffusion propagator [1–3]. The representation (6) of the macroscopic signal is called the narrow pulse approximation. Its validity has been thoroughly investigated numerically and experimentally, while the NPA has become one of the central theoretical approaches for analysis and interpretation of experimental dMRI measurements [86–92].

From theoretical point of view, it is also convenient to consider the local contribution to the PGSE signal of the nuclei started from a fixed point y:

$$\widetilde{M}(y) = \int_{-\infty}^{\infty} dx e^{iq(x-y)}G(x,y;\Delta). \quad (7)$$

The PGSE signal S is retrieved by integrating $\widetilde{M}(y)$ with the initial density $\rho(y)$. Though being inaccessible experimentally, the local contribution $\widetilde{M}(y)$ helps to understand the role of diffusion from different starting points.

Substituting Eq. (5) and assuming $y > 0$, we obtain after lengthy but straightforward integration

$$\widetilde{M}(y) = e^{-\tilde{q}^2} + \widetilde{M}_b(y), \quad (8)$$

where

$$\widetilde{M}_b(y) = \frac{e^{-\tilde{y}^2-2i\tilde{y}\tilde{q}}}{2(\tilde{q}^2+\tilde{\kappa}^2)}\left(\tilde{q}^2[w(i\tilde{y}+\tilde{q}) - w(i\tilde{y}-\tilde{q})] + i\tilde{q}\tilde{\kappa}[w(i\tilde{y}-\tilde{q}) + w(i\tilde{y}+\tilde{q}) - 2w(i\tilde{y}+i\tilde{\kappa})]\right), \quad (9)$$

$\tilde{y} = y/\sqrt{4D\Delta}, \tilde{q} = q\sqrt{D\Delta}, \tilde{\kappa} = 2\kappa\sqrt{\Delta/D}$ are dimensionless quantities, and $w(z) \equiv e^{-z^2}\operatorname{erfc}(-iz)$ is the Faddeeva function. For negative starting points $y < 0$, one gets $\widetilde{M}_b(y) = \widetilde{M}_b^*(-y)$, where asterisk denotes complex conjugate.

The local contribution $\widetilde{M}(y)$ has a constant term $e^{-\tilde{q}^2}$ corresponding to unrestricted diffusion (without barrier), and the barrier contribution $\widetilde{M}_b(y)$ which rapidly decays as $y \to \pm\infty$: $\widetilde{M}_b(y) \propto \exp(-y^2/(4D\Delta))$. In the limit $\kappa \to \infty$, the barrier disappears, and one retrieves $\widetilde{M}_0(y) = e^{-\tilde{q}^2} = \exp(-D\gamma^2 g^2\delta^2\Delta)$, as expected for unrestricted diffusion. It is worth noting that the integral of $\widetilde{M}(y)$ over the starting points y on the whole line diverges due to the constant term $e^{-\tilde{q}^2}$ that required the introduction of the initial density $\rho(y)$.

If the initial magnetization is uniformly distributed over an interval $[-R,R]$, the signal under the NPA can be written as

$$S = \frac{1}{2R}\int_{-R}^{R} dy\widetilde{M}(y) = e^{-\tilde{q}^2} + S_b, \quad (10)$$

where the barrier signal is

$$S_b = \frac{1}{2R}\int_{-R}^{R} dy\widetilde{M}_b(y) \simeq \frac{1}{2R}\int_{-\infty}^{\infty} dy\widetilde{M}_b(y) = \frac{\sqrt{D\Delta}}{2R}s_b, \quad (11)$$

with

$$s_b = \frac{2\tilde{q}^2}{\sqrt{\pi}(\tilde{q}^2+\tilde{\kappa}^2)}\left[-1 + (1+2\tilde{q}^2)\frac{\mathcal{D}(\tilde{q})}{\tilde{q}} + \sqrt{\pi}\tilde{\kappa}e^{-\tilde{q}^2} - \frac{2\tilde{\kappa}^2\mathcal{D}(\tilde{q})}{\tilde{q}(\tilde{q}^2+\tilde{\kappa}^2)} + \frac{\sqrt{\pi}\tilde{\kappa}}{\tilde{q}^2+\tilde{\kappa}^2}\left(e^{-\tilde{q}^2} - e^{\tilde{\kappa}^2}\operatorname{erfc}(\tilde{\kappa})\right)\right], \quad (12)$$

and

$$\mathcal{D}(\tilde{q}) \equiv e^{-\tilde{q}^2}\int_0^{\tilde{q}} dz e^{z^2} = -\frac{i\sqrt{\pi}}{2}\operatorname{erf}(i\tilde{q})e^{-\tilde{q}^2} \quad (13)$$

is the Dawson function. Note that the error related to the extension of the integral in Eq. (11) from $[-R,R]$ to $[-\infty,\infty]$ is negligible if $R \gg \sqrt{2D\Delta}$. We emphasize that the barrier signal S_b and thus the total signal S depend on the initial distribution (in particular, on R). In contrast to the signal from unrestricted diffusion which depends on the single parameter $\tilde{q}$, the barrier signal depends on three parameters: the dimensionless strength of gradient encoding

[1] For shorter notations, we do not write the factor $1/(2\pi)$ which is included in the standard definition of q. This omission does not affect any quantitative conclusion.

$\tilde{q}$, the dimensionless permeability $\tilde{\kappa}$, and the dimensionless density $\sqrt{D\Delta}/(2R)$. Note that at small $\tilde{\kappa}$, one gets

$$s_b = \frac{2}{\sqrt{\pi}}((2\tilde{q}+1/\tilde{q})\mathcal{D}(\tilde{q})-1) - \frac{4\kappa}{D}\sqrt{D\Delta}\frac{1-(\tilde{q}^2+1)e^{-\tilde{q}^2}}{\tilde{q}^2} + O(\tilde{\kappa}^2), \quad (14)$$

i.e., the next-order correction in the diffusion length $\sqrt{D\Delta}$ is proportional to the permeability. In the opposite limit of large κ, one has $s_b \simeq 2\tilde{q}^2 e^{-\tilde{q}^2}/\tilde{\kappa}$, and the barrier signal vanishes as $1/\kappa$.

The above analysis relies on the explicit form (5) of the propagator $G(x,y;t)$ for a single semi-permeable barrier. Although an exact extension to multiple barriers might formally be obtained, its practical use would be limited. At the same time, the rapid decay of $\widetilde{M}_b(y)$ with y allows one to apply the same formulas to multiple *well-separated* barriers. In fact, if the inter-barrier distance (i.e., the distance between any two adjacent barriers) is much larger than the diffusion length, the nuclei diffusing near one barrier are not influenced by the neighboring barriers. For instance, if the voxel of size $2R$ contains n well-separated barriers, the signal under the NPA reads

$$S \approx \exp(-D(\gamma g\delta)^2\Delta) + \frac{\sqrt{D\Delta}}{\ell_b}s_b, \quad (15)$$

where $\ell_b = 2R/n$ is the average inter-barrier distance. Here, we assumed that all the barriers have the same permeability so that each of them provided the same contribution. If barriers have different permeabilities, one takes the sum of the related contributions. Fitting the acquired PGSE signal to the above theoretical formula allows one to estimate the permeability κ and the averaged distance ℓ_b between the barriers (see below).

2.3. Impermeable barrier

We first consider the case $\kappa = 0$, for which Eq. (12) is reduced to the formula found in [93]:

$$s_b = \frac{2}{\sqrt{\pi}}((2\tilde{q}+1/\tilde{q})\mathcal{D}(\tilde{q})-1). \quad (16)$$

Setting the derivative of this function with respect to $\tilde{q}$ to zero yields the equation

$$\mathcal{D}(\tilde{q}_c) = \frac{2\tilde{q}_c(1+2\tilde{q}_c^2)}{1+4\tilde{q}_c^4} \quad (17)$$

on the optimal value $\tilde{q}_c$, from which

$$\tilde{q}_c = 1.1745\ldots \quad (18)$$

or, equivalently,

$$g_{\rm opt} = \frac{1.1745}{\gamma\delta\sqrt{D\Delta}}, \quad (19)$$

at which the barrier signal S_b is maximal for a given diffusion time Δ, with $s_b(\tilde{q}_c) \simeq 0.7229$ (Fig. 1). Note that the contribution $e^{-\tilde{q}^2}$ from unrestricted diffusion takes the value 0.2517 at $\tilde{q} = \tilde{q}_c$. As a consequence, the signal at the optimal gradient is

$$S \approx 0.2517 + 0.7229\frac{\sqrt{D\Delta}}{\ell_b}. \quad (20)$$

We remind that this expression is valid under condition that the barriers are well separated: $\ell_b \gg \sqrt{D\Delta}$.

The adaptive variation of the gradient with the diffusion time according to Eq. (19) results in a *constant* b-value (the quantity which is used in dMRI experiments to characterize diffusion-encoding gradient profile). In fact, for narrow gradient pulses, one has $b = \gamma^2 g^2 \delta^2 \Delta = \tilde{q}^2/D$, and if $\tilde{q}$ is fixed at $\tilde{q}_c$, then $bD = \tilde{q}_c^2 \approx 1.38$. This protocol is drastically different from the conventional dMRI, in which the b-value is varied either by increasing the gradient g at fixed diffusion time Δ, or by increasing the diffusion time at fixed gradient. In particular, most dMRI studies of brain tissues focused on apparent diffusion coefficient which is obtained from the signal at small b-values. In our approach, the b-value is fixed at the optimal value to ensure the maximal contribution from the barrier.

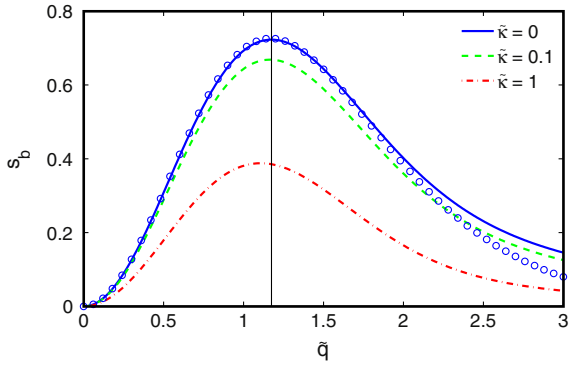

Fig. 1. The barrier contribution s_b from Eq. (12) as a function of the dimensionless wave vector $\tilde{q}$ for different dimensionless permeabilities $\tilde{\kappa}$. Vertical black line indicates the position $\tilde{q}_c = 1.1745$ of the maximum for $\tilde{\kappa} = 0$. Circles present the approximation (22) that we derived from Ref. [94].

It is instructive to compare our result to the earlier study of the PGSE signal from water molecules diffusing between two impermeable barriers [94]. In this work, Sukstanskii et al. showed that the PGSE signal in the short-time limit could be accurately modeled by a biexponential function:

$$S \simeq \zeta\exp(-bD_1) + (1-\zeta)\exp(-bD_2), \quad (21)$$

where $D_1 \simeq 0.30D, D_2 \simeq D(1-0.35\alpha)$, and $\zeta \simeq 0.59\alpha$ if $\alpha = 2\sqrt{D\Delta}/\ell_b \ll 1$. The first-order expansion of Eq. (21) in terms of α yields Eq. (15), with

$$s_b \simeq 1.18(e^{-0.3\tilde{q}^2} - e^{-\tilde{q}^2}) + 0.70\tilde{q}^2 e^{-\tilde{q}^2}, \quad (22)$$

where we replaced bD by $\tilde{q}^2$. As illustrated on Fig. 1, this is an excellent approximation to the exact formula (16).

We conclude this subsection by mentioning the series of works by Mitra et al. who investigated the PGSE signal in porous media in the short-time limit [57–61]. In their asymptotic formula for the time-dependent diffusion coefficient, $D(\Delta) \simeq D(1 - \frac{4S_p}{3d\sqrt{\pi}V_p}\sqrt{D\Delta} + \ldots)$, the first-order correction comes from the nuclei in the surface layer of width $\sqrt{D\Delta}$, where S_p/V_p is the surface-to-volume ratio, and d the space dimension. At small gradients, the PGSE signal can be approximated as $e^{-bD(\Delta)}$, from which one gets (see also [3])

$$S \simeq e^{-\tilde{q}^2} + \sqrt{D\Delta}\frac{4S_p}{3d\sqrt{\pi}V_p}\tilde{q}^2 e^{-\tilde{q}^2} + \ldots$$

As earlier, one can interpret the second term as the barrier (or surface) contribution. However, this asymptotic relation is only valid for small gradients (i.e., small $\tilde{q}$), at which the contribution from unrestricted diffusion (the first term) dominates. We emphasize that our protocol with an optimal constant b-value is not reducible to the analysis of apparent diffusion coefficients at small b-values.

2.4. Multiple impermeable barriers

When the voxel contains multiple impermeable barriers (with $\kappa = 0$), the PGSE signal is the weighted sum of signals $S_{1d}(L_n)$ from each interval between two adjacent (reflecting) barriers:

$$S = \sum_{n=1}^{N}\frac{L_n}{L_{\rm tot}}S_{1d}(L_n), \quad (23)$$

where L_n is the length of the nth interval, $L_{\rm tot} = L_1 + \cdots + L_N$ is the total length, and $L_n/L_{\rm tot}$ is the "volume" fraction. The signal $S_{1d}(L)$ from the nuclei confined into an isolated interval $[0, L]$ with two reflecting endpoints is well known under the NPA [85]:

$$S_{1d}(L) = 2(qL)^2 \sum_{m=0}^{\infty} \varepsilon_m^2 e^{-D\lambda_m \Delta/L^2} \frac{1-(-1)^m \cos(qL)}{\left[\lambda_m - (qL)^2\right]^2}, \qquad (24)$$

where $\lambda_m = \pi^2 m^2, \varepsilon_m = \sqrt{2}$ for $m > 0$, and $\varepsilon_0 = 1$. When the gradient (or q) is varied with Δ according to Eq. (19), the signal $S_{1d}(L)$ is a function of a single dimensionless variable $\sqrt{D\Delta}/L$. In the long-time limit $\sqrt{D\Delta}/L \to \infty$, one gets $S_{1d}(L) = 1$. The opposite short-time limit is equivalent to our analysis of a single impermeable barrier on the whole line, for which the signal is given by Eq. (20) with $\ell_b = L$. Fig. 2 illustrates an excellent agreement between the classical NPA signal (shown by circles) from Eq. (24) and our prediction Eq. (20) (shown by line).

When the lengths L_n are identical (or close to each other), $L_n = L$, the total signal is equal to $S_{1d}(L)$, and fitting the signal to Eq. (20) allows one to estimate the inter-barrier distance. In contrast, if some lengths are much smaller than the others, one can get their contributions by varying the diffusion length $\sqrt{D\Delta}$. For instance, for two intervals with lengths L_1 and L_2 such that $L_1 \ll L_2$, two limits are expected. When $\sqrt{D\Delta} \ll L_1$, one gets

$$S \simeq 0.2517 + 0.7229 \frac{\sqrt{D\Delta}}{\ell_b}, \qquad \ell_b = \frac{1}{2}(L_1 + L_2), \qquad (25)$$

while for $L_1 \ll \sqrt{D\Delta} \ll L_2$, one gets

$$S \simeq \frac{L_1}{L_1 + L_2} + \frac{L_2}{L_1 + L_2}\left[0.2517 + 0.7229 \frac{\sqrt{D\Delta}}{L_2}\right], \qquad (26)$$

where the first term is the weighted contribution from the short interval (with the corresponding signal equal to 1), and the second term is the weighted contribution from the long interval. Fig. 3 illustrates the transition between these limits when $\sqrt{D\Delta}$ is changed. As a consequence, varying the diffusion length, one can potentially probe various inter-barrier distances.

2.5. Isolated disk and sphere

The signal for an isolated disk (or cylinder) of radius L under the NPA is also well known [87]:

$$S_{2d} = 4(qL)^2 \sum_{n,k=0}^{\infty} e^{-D\lambda_{nk}\Delta/L^2} \frac{\varepsilon_n^2 \lambda_{nk}}{\lambda_{nk} - n^2} \frac{\left[J_n'(qL)\right]^2}{\left[\lambda_{nk} - (qL)^2\right]^2}, \qquad (27)$$

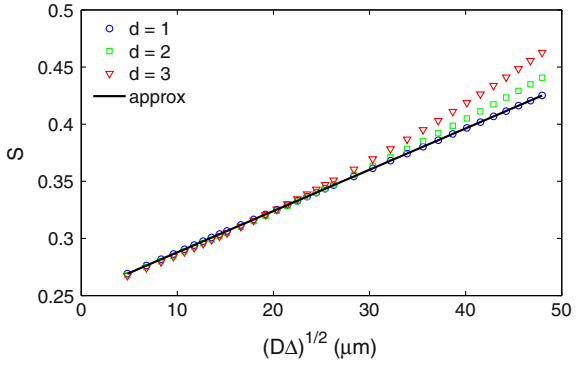

Fig. 2. PGSE signal S (shown by symbols) for isolated interval of length $2L$ [circles, Eq. (24)], disk of radius L [squares, Eq. (27)], and sphere of radius L [triangles, Eq. (28)]. The signal is computed as a function of the diffusion length $\sqrt{D\Delta}$, when the gradient g is varied adaptively with Δ according to Eq. (19). We set $D = 2.3 \cdot 10^{-9}$ m^2/s, $L = 100$ μm. The initial magnetization is set uniformly. For comparison, black solid line presents the approximation (20).

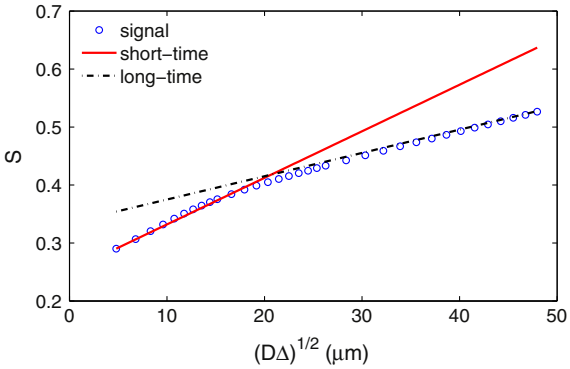

Fig. 3. PGSE signal S (shown by symbols) from Eq. (23) for a multilayered structure composed of isolated intervals of lengths $L_1 = 20$ μm and $L_2 = 80$ μm (the case $\kappa = 0$). The signal is computed as a function of the diffusion length $\sqrt{D\Delta}$, when the gradient g is varied adaptively with Δ according to Eq. (19). We set $D = 2.3 \cdot 10^{-9}$ m^2/s. The initial magnetization is set uniformly. For comparison, red solid line presents the short-time approximation (25), while black dash-dotted line shows the long-time approximation (26).

where $J_n'(z)$ is the derivative of the Bessel function of the first kind, and $\sqrt{\lambda_{nk}}$ are the positive roots of the equation $J_n'(z) = 0$ $(n = 0, 1, 2, \ldots)$, enumerated by an index $k = 0, 1, 2, \ldots$ Note that $\lambda_{0,0} = 0$, and the ratio $\lambda_{nk}/(\lambda_{nk} - n^2)$ is set to 1 for $n = k = 0$.

Similarly, the signal for an isolated sphere of radius L is

$$S_{3d} = 6(qL)^2 \sum_{n,k=0}^{\infty} e^{-D\lambda_{nk}\Delta/L^2} \frac{(2n+1)\lambda_{nk}}{\lambda_{nk} - n(n+1)} \frac{\left[j_n'(qL)\right]^2}{\left[\lambda_{nk} - (qL)^2\right]^2}, \qquad (28)$$

where $j_n'(z)$ is the derivative of the spherical Bessel function, and $\sqrt{\lambda_{nk}}$ are the positive roots of the equation $j_n'(z) = 0$ $(n = 0, 1, 2, \ldots)$, enumerated by an index $k = 0, 1, 2, \ldots$ Note that $\lambda_{0,0} = 0$, and the ratio $\lambda_{nk}/(\lambda_{nk} - n(n+1))$ is set to 3/2 for $n = k = 0$.

These signals are plotted on Fig. 2 for a disk (shown by squares) and a sphere (shown by triangles). For small diffusion length $\sqrt{D\Delta}$, both signals are accurately approximated by Eq. (20). At larger $\sqrt{D\Delta}$, some deviations appear due to the fact that the nuclei diffusing inside a disk or a sphere experience variable restriction lengths.

2.6. Single permeable barrier

When $\kappa > 0$, the barrier signal S_b from Eqs. (11) and (12) also exhibits a maximum. In fact, the total signal approaches 1 at small gradients due to normalization. As the contribution from unrestricted diffusion, $e^{-\tilde{q}^2}$, also approaches 1, the barrier signal S_b vanishes at $\tilde{q} = 0$. Since the total signal is strongly attenuated at large gradients (i.e., $\tilde{q} \to \infty$), the barrier signal should exhibit a maximum. Although there is no simple formula for the value q_c, Fig. 1 illustrates that q_c weakly depends on the permeability: while the height of the maximum decreases with κ, its horizontal position remains almost the same. Moreover, we checked numerically that q_c slowly decreases from 1.1745 at $\tilde{\kappa} = 0$ to 1 at $\tilde{\kappa} \to \infty$. As a consequence, the optimal gradient from Eq. (19) can be used for permeable barriers as well.

Since our approach relies on the assumption of infinitely narrow gradient pulses, we start by comparing theoretical formulas (10)–(12) to the PGSE signal computed for rectangular gradient pulses of small but finite duration $\delta = 0.5$ ms. For this purpose, we compute the signal from the nuclei diffusing in the interval $[-L, L]$ $(L = 200$ μm), with two reflecting endpoints and a single semi-permeable barrier at the origin with the permeability κ. In order to reduce the effects of reflecting endpoints, the initial magnetization was distributed uniformly over the subinterval $[-R, R] \subset [-L, L]$, with $R = 100$ μm. The gradient intensity g was

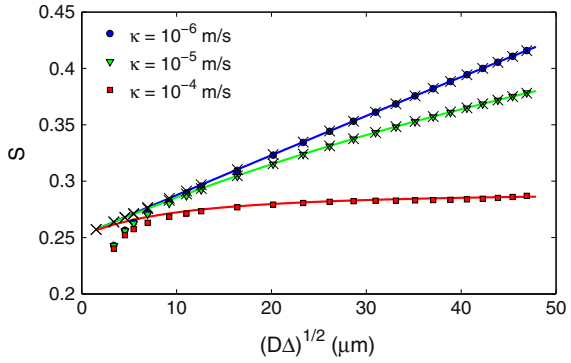

Fig. 4. PGSE signal S (shown by symbols) for an interval $[-L, L]$ with two reflecting endpoints and a semi-permeable barrier at the origin, with different permeabilities κ. The signal is computed as a function of the diffusion length $\sqrt{D\Delta}$, when the gradient g is varied adaptively with Δ according to Eq. (19). We set $L = 200$ μm, $\delta = 0.5$ ms, $D = 2.3 \cdot 10^{-9}$ m^2/s, and the initial magnetization is set uniformly over the subinterval $[-R, R]$, with $R = 100$ μm. For comparison, solid lines present the one-barrier approximation (15), with s_b from Eq. (12). At low permeability, one retrieves a linear dependence on $\sqrt{D\Delta}$ according to Eq. (20), with $\ell_b = 2R$. Crosses indicate the signals obtained from the asymptotic relation (14) for s_b which yields accurate results for small and intermediate permeabilities but fails at high permeability $\kappa = 10^{-4}$ m/s (not shown).

varied adaptively with Δ according to Eq. (19). The signal was computed by the matrix formalism (see Appendix A).

As discussed in Section 1, the water permeability κ can vary in a broad range, from 10^{-8} m/s to almost 10^{-4} m/s. The permeability appears in the barrier signal S_b in Eq. (12) through the dimensionless parameter $\tilde{\kappa} = 2\kappa\sqrt{\Delta/D}$, which naturally determines the characteristic scale $\kappa_\Delta = \frac{1}{2}\sqrt{D/\Delta}$. For diffusion times Δ from 10 ms to 1 s, κ_Δ varies from $2.4 \cdot 10^{-4}$ m/s to $2.4 \cdot 10^{-5}$ m/s. In what follows, we consider three values of κ, 10^{-6} m/s, 10^{-5} m/s, and 10^{-4} m/s, that we conventionally refer to as low, intermediate, and high permeability.

Fig. 4 presents the computed PGSE signals (shown by symbols) and our approximation (15) (shown by lines). The diffusion time Δ varied from 1 ms to 1 s that is equivalent to variations of the diffusion length $\sqrt{D\Delta}$ from several to fifty microns (the range of the horizontal axis). At very small Δ, the assumption $\delta \ll \Delta$ of the NPA does not hold that results in deviations. Starting from $\sqrt{D\Delta} \sim 10$ μm, Eq. (15) accurately approximates the computed signals for all considered permeabilities. At low permeability ($\kappa = 10^{-6}$ m/s), the signal exhibits almost linear dependence on $\sqrt{D\Delta}$, as predicted by Eq. (20) with $\ell_b = 2R$ (here, a single barrier is present for the initial magnetization extended over the length $2R$). The explicit form and the accuracy of the approximation (15) suggest to use this expression to fit PGSE signals and thus estimate the permeability κ. We also present by crosses the results of using the small-$\tilde{\kappa}$ asymptotic relation (14) which accurately approximates s_b from the exact formula (12) for small and intermediate permeabilities but fails at high permeability $\kappa = 10^{-4}$ m/s.

2.7. Multiple periodic permeable barriers

Sukstanskii et al. derived an exact solution of the one-dimensional model with periodic permeable barriers under the narrow pulse approximation [25]. For this configuration, they provided explicit formulas for the magnetization and the signal, as well as a thorough analysis of their asymptotic behaviors at short and long times. In particular, the signal admits the following spectral representation

$$S = \frac{2(qL)^2}{\kappa L/D} \sum_{n=0}^{\infty} \frac{e^{-D\alpha_n^2 \Delta/L^2} \alpha_n^2 \sin(\alpha_n)}{\left[(qL)^2 - \alpha_n^2\right]^2 \left[\left(\frac{2\kappa L}{D} + 1\right) \sin\alpha_n + \alpha_n \cos\alpha_n\right]}, \qquad (29)$$

where $L = \ell_b$ is the inter-barrier distance, and α_n denote all positive solutions of the equation

$$\frac{2\kappa L}{D}(\cos\alpha - \cos(qL)) - \alpha \sin\alpha = 0. \qquad (30)$$

In the short-time limit, Eq. (29) is reduced to Eq. (10) for a single semi-permeable barrier.[2] We used the exact solution in Eq. (29) in order to check the accuracy of our approximation when $\sqrt{D\Delta} \ll L$ (not shown).

It is worth emphasizing that the method from Ref. [25] relies on the periodic arrangement of infinitely many barriers, i.e., on the assumption of identical inter-barrier distances. In contrast, our single-barrier approximation (or, equivalently, the short-time behavior of Eq. (29)) is applicable to arbitrary arrangement of barriers, if they are well separated on the scale of the diffusion length.

2.8. Multiple permeable barriers

Finally, we consider a multilayered structure with two reflecting endpoints and four semi-permeable barriers (each with permeability κ) separated by equal distances ℓ_b. Fig. 5 shows the PGSE signal as a function of the diffusion length $\sqrt{D\Delta}$ when the gradient g is varied adaptively with Δ according to Eq. (19). The PGSE signals were computed by the matrix formalism for multilayered structures [24], with the pulse duration $\delta = 0.5$ ms. The initial magnetization is set uniformly over the three intermediate layers, in order to reduce the effect of reflecting endpoints. The permeability was ranged from $\kappa = 10^{-6}$ m/s (almost impermeable barrier) to $\kappa = 10^{-4}$ m/s (almost fully permeable barrier).

When the inter-barrier distance ℓ_b is large (Fig. 5a, $\ell_b = 160$ μm), the approximation (15) accurately reproduces the PGSE signals for all permeabilities and diffusion times up to one second. At low permeability $\kappa = 10^{-6}$ m/s, the linear dependence (20) of the signal on the diffusion length $\sqrt{D\Delta}$ is clearly seen. At higher permeabilities, the barrier signal diminishes.

For smaller inter-barrier distances (Fig. 5b for $\ell_b = 80$ μm and Fig. 5c for $\ell_b = 40$ μm), the validity range of the approximation (15) is narrower. In fact, this approximation holds when $\sqrt{D\Delta} \ll \ell_b$, while deviations emerge at longer diffusion lengths. The failure of the approximation (15) at long times is particularly clear from Fig. 5c, on which the predicted signal attenuation exceeds 1 at large $\sqrt{D\Delta}$, while the computed PGSE signal saturates to 1, as expected.

3. Application to three-dimensional domains

The above analysis relied on the one-dimensional diffusion propagator from which explicit formulas of the PGSE signal were derived. These formulas are applicable to an array of parallel planes as the problem remains one-dimensional. However, biological tissues are typically composed of compact cells of variable shapes which are separated from the extracellular space by semi-permeable cellular membranes. For such domains, one needs to resort to numerical methods for computing the diffusion propagator and the PGSE signal. Although the above analysis is formally not applicable in such more general situation, the concept of adaptive change of the gradient intensity with the diffusion time can still be valuable to enhance the barrier contribution.

In order to illustrate this point, we first consider a specific domain in which cells form "columns" in one direction (Fig. 6a). When the gradient is oriented along these columns while the exchange between the cells in columns is slow, the signal is simply

[2] Note that this limit was also derived by Sukstanskii et al., but there was a misprint in Eq. (A.1) of Ref. [25].

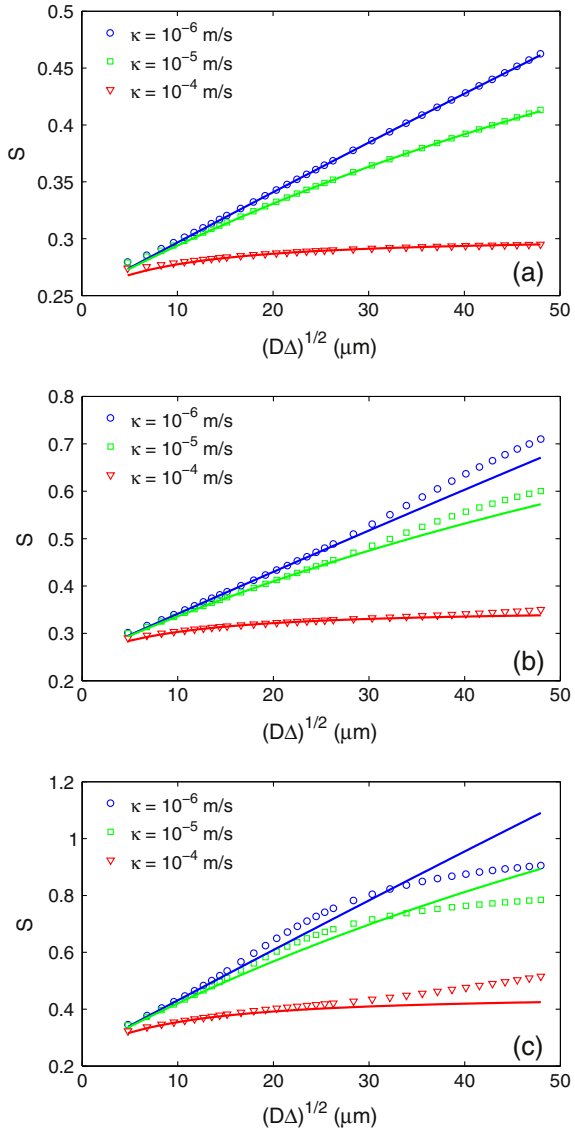

Fig. 5. PGSE signal S (shown by symbols) for a 5-layered structure with two reflecting endpoints and four semi-permeable barriers (each with permeability κ) separated by equal distances ℓ_b. The signal is computed as a function of the diffusion length $\sqrt{D\Delta}$, when the gradient g is varied adaptively with Δ according to Eq. (19). We set $\delta = 0.5$ ms, $D = 2.3 \cdot 10^{-9}$ m^2/s, and three values of ℓ_b: 160 μm (a), 80 μm (b), and 40 μm (c). The initial magnetization is set uniformly over the three intermediate layers. For comparison, solid lines present our approximation (15). At low permeability, one retrieves a linear dependence on $\sqrt{D\Delta}$ according to Eq. (20).

a weighted sum of signals from the extracellular space (unrestricted diffusion) and from these "columns":

$$S = (1 - v_c)S_0 + v_c(S_0 + S_b) = S_0 + s_b v_c \frac{\sqrt{D\Delta}}{\ell_b}, \tag{31}$$

where v_c is the volume fraction of cells, S_0 is the signal from unrestricted diffusion, and S_b is the barrier signal that effectively accounts for exchange between cells and the extracellular space. This relation can be used to estimate the ratio v_c/ℓ_b from the signal:

$$\frac{\ell_b}{v_c} = 0.7229 \frac{\sqrt{D\Delta}}{S - S_0}, \tag{32}$$

where we used Eq. (20) for impermeable barriers, and $S_0 = 0.2517$ at the optimal gradient setting.

In a general configuration, cells are placed irregularly in the extracellular space, while the exchange across the cellular membranes can be significant. As a consequence, Eq. (31) is not necessarily valid. In order to check this point, we consider two three-dimensional domains: an array of periodically placed cubes of size $2R$ (Fig. 6b), and an array of periodically placed spheres of radius R (Fig. 6c). In both cases, the centers of cells are separated by distance $L = 100$ μm. For these configurations, the Bloch–Torrey equation with standard interface conditions at semi-permeable membranes was solved numerically by a finite elements method [69]. The periodic arrangement of cells was modeled by setting periodic boundary conditions on the exterior boundary of the computational domain. The standard PGSE sequence with two rectangular pulses of duration $\delta = 0.5$ ms was implemented. The computation was performed for water diffusion coefficient $D = 2.3 \cdot 10^{-9}$ m^2/s and three permeabilities: $\kappa = 10^{-6}$ m/s, $\kappa = 10^{-5}$ m/s, and $\kappa = 10^{-4}$ m/s. The signal S was computed by varying adaptively the gradient intensity g and the diffusion time Δ according to Eq. (19). The gradient was oriented as $[1, 0, 0]$ for these computations while similar results were obtained for other gradient directions (not shown).

Fig. 7 shows the effective inter-barrier distance ℓ_b computed from Eq. (32), where we set $v_c = (2R/L)^3$ for cubic cells, and $v_c = \frac{4\pi}{3}(R/L)^3$ for spherical cells. By construction, ℓ_b would be independent of the diffusion length $\sqrt{D\Delta}$ and equal to the inter-barrier distance for impermeable equidistant one-dimensional barriers. In contrast, Fig. 7 illustrates an increase of this effective parameter with $\sqrt{D\Delta}$ for cubic and spherical cells. Nevertheless, for small permeability $\kappa = 10^{-6}$ m/s (Fig. 7a), one can clearly distinguish an extended plateau for $\sqrt{D\Delta}$ between 10 μm and 20–40 μm. The height of this plateau is close to the size R of cells (indicated by horizontal thin lines). Probing the effective inter-barrier distance (obtained by Eq. (32) from the PGSE signal) can potentially be used to estimate the size of cells. Note that the plateau is more distinct

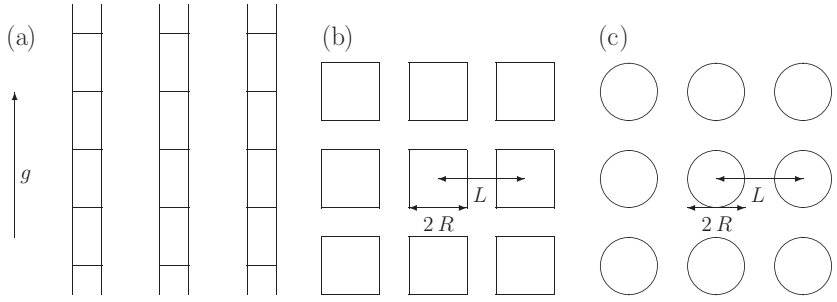

Fig. 6. Schematic two-dimensional illustration of three configurations of cells: (a) rectangular cells forming columns in one direction; (b) array of cubic cells of size $2R$; and (c) array of spherical cells of radius R.

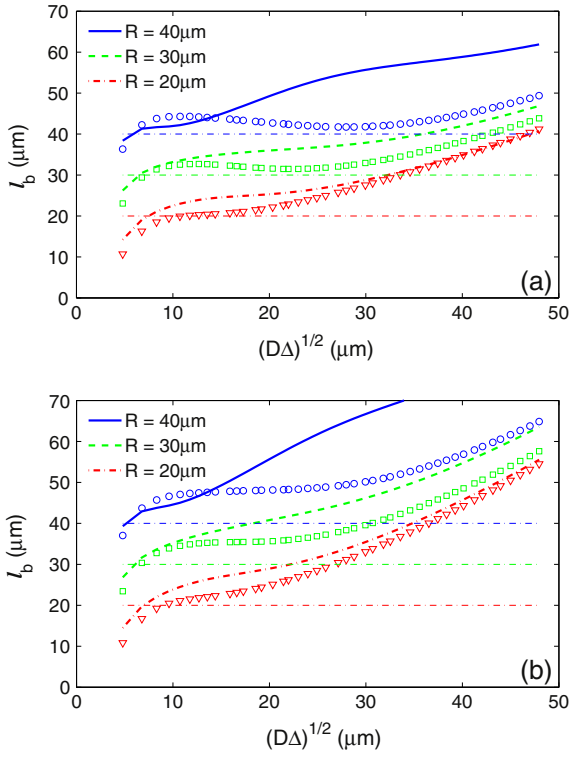

Fig. 7. Effective inter-barrier distance ℓ_b computed according to Eq. (32) from the simulated PGSE signal S for an array of cubes of size $2R$ (lines) and for an array of spheres of radius R (symbols), separated by distance $L = 100$ μm. The signal is computed as a function of the diffusion length $\sqrt{D\Delta}$, when the gradient g is varied adaptively with Δ according to Eq. (19). We set $\delta = 0.5$ ms, $D = 2.3 \cdot 10^{-9}$ m^2/s, and $\kappa = 10^{-6}$ m/s (a) and $\kappa = 10^{-5}$ m/s (b). For small $\sqrt{D\Delta}$, the effective inter-barrier distance is close to the size R of cells (shown by horizontal dotted lines).

for spherical cells (data shown by symbols). For higher permeability $\kappa = 10^{-5}$ m/s (Fig. 7b), one can still distinguish a plateau for spherical cells while ℓ_b monotonously grows for cubic cells. The height of the plateau overestimates the size of spherical cells by 10–20%. Finally, Eq. (32) becomes invalid for large permeability $\kappa = 10^{-4}$ m/s (not shown). In that case, the barrier contribution S_b cannot be approximated by Eq. (20) which was originally derived for impermeable barriers. If the permeability is known, the exact formula (12) could be used instead of Eq. (20). In general, when the permeability is not known *a priori*, Eq. (12) can be used to estimate both the permeability and the inter-barrier distance by fitting the PGSE signal acquired at variable diffusion times and gradients but fixed (optimal) b-value.

These preliminary results suggest that the use of adaptive variation of the gradient intensity and the diffusion time can be useful for three-dimensional domains. In fact, the barrier (or surface) contribution S_b is still proportional to the diffusion length $\sqrt{D\Delta}$ at short times, and S_b as a function of the dimensionless wave vector $\tilde{q}$ should have a maximum (the simple argument from Section 2.6 remains valid in general). However, the optimal value $\tilde{q}_c$ and the proportionality coefficient s_b in Eq. (15) are geometry-dependent. In order to evaluate these parameters, one can decompose the applied gradient $\mathbf{g}$ at each boundary point into two components $\mathbf{g}_\parallel$ and $\mathbf{g}_\perp$ which are parallel and perpendicular to the boundary. If the boundary $\partial\Omega$ is smooth (i.e., the radius of curvature is much larger than the diffusion length), the local signal attenuation has two contributions: from parallel motion (unrestricted diffusion) and from perpendicular motion, for which the one-dimensional contribution s_b can be used. Under these approximations, the signal is obtained by integrating local contributions from all boundary points:

$$S \simeq e^{-\tilde{q}^2} + \frac{\sqrt{D\Delta}}{L^d} \int_{\partial\Omega} d\mathbf{s} e^{-\tilde{q}^2 \sin^2\theta(\mathbf{s})} s_b(\tilde{q}\cos\theta(\mathbf{s})), \tag{33}$$

where $\theta(\mathbf{s})$ is the angle between the gradient direction and the normal vector at the boundary point $\mathbf{s}$, $e^{-\tilde{q}^2\sin^2\theta(\mathbf{s})}$ is the attenuation factor from unrestricted diffusion in direction parallel to the boundary (note that $\tilde{q}^2 = bD$), $\tilde{q}\cos\theta(\mathbf{s})$ is the dimensionless wave vector in the perpendicular direction, and the uniform initial distribution was assumed over the cubic voxel of size L in d dimensions. Since the general formula (12) for s_b is too complicated for integration, one can use the approximate Eq. (22) for impermeable barriers. For instance, for a sphere of radius R, one gets

$$S \simeq e^{-\tilde{q}^2} + v_c \frac{\sqrt{D\Delta}}{R} s_b^{\text{sphere}}, \tag{34}$$

where

$$s_b^{\text{sphere}} \simeq 4.23 e^{-0.3\tilde{q}^2} \frac{\mathcal{D}(0.84\tilde{q})}{\tilde{q}} - 3.54 e^{-\tilde{q}^2} + 0.70\tilde{q}^2 e^{-\tilde{q}^2}. \tag{35}$$

This function exhibits a maximum 0.6448 at $\tilde{q}_c \approx 1.08$, i.e., these values are close to the parameters $s_b = 0.7229$ and $\tilde{q}_c = 1.1745$ for one-dimensional barriers. It explains why the one-dimensional approach yielded a reasonably good estimation of the size of spherical cells on Fig. 7. Further numerical analysis is needed to make this protocol operational for more complicated shapes and configurations of cells.

From a practical point of view, the major limitation of the present approach is the condition on the inter-barrier distance to be large as compared to the diffusion length. Even for diffusion times Δ as short as few milliseconds, the diffusion length for water molecules is few microns that is comparable to the size of cells in most biological tissues in humans and animals. In this situation, cell membranes cannot be considered as well separated, and formulas derived for a single barrier are not applicable. Nevertheless, the principal idea of maximizing the barrier contribution by varying adaptively the gradient and the diffusion time can still be fruitful. As a perspective, extending this approach to oscillating gradients can probably reduce such limitations. At the same time, the present approach can be applied to study water exchange in plants because plant cells are much larger than animal cells, and their spatial arrangements are often quite regular [81].

4. Conclusion

We studied a simplified problem of one-dimensional diffusion across permeable barriers. In dMRI, one often resorts to one-dimensional models by basically two reasons: (i) drastic simplifications of the underlying mathematics in one dimension; and (ii) water diffusion in three-dimensional samples is still probed along one direction (of the applied gradient). Although the transverse diffusion may strongly affect the signal, some qualitative and even quantitative insights from one-dimensional models are still valuable.

For the basic model of a single semi-permeable barrier on a line, we obtained an exact simple representation of the PGSE signal in the frame of the narrow pulse approximation. This representation contained the classical contribution from unrestricted diffusion, and the barrier contribution. We showed that the barrier signal exhibits a maximum so that varying the gradient adaptively with the diffusion time Δ can enhance the contribution from the barrier signal at each Δ and thus facilitate the determination of the inter-barrier distance and permeability. Such adaptive variation suggests a new dMRI protocol at an optimal constant b-value, in contrast to conventional dMRI in which the PGSE signal is acquired as a function of b-value. At low permeability, the PGSE signal was shown to

be linearly proportional to the diffusion length $\sqrt{D\Delta}$, from which the inter-barrier distance can be determined. At higher permeabilities, this linear dependence is progressively reduced due to rapid exchange across the barrier. For multiple barriers that are well separated on the diffusion length, the adaptive variation of the gradient with the diffusion time allows one to probe various inter-barrier distances.

Finally, we showed that the new protocol which was mathematically developed for one-dimensional diffusion, is also applicable to three-dimensional configurations of cells. First, we checked that the classical formulas for the PGSE signal from the NPA for isolated cylinders and isolated spheres exhibit the same features as its one-dimensional counterpart. Second, we solved numerically the Bloch–Torrey equation for periodically placed spherical and cubic cells by a finite elements method. Formally applying the one-dimensional theory, we managed to estimate the cell radius, at least at low permeability. This approach can be applied to study water exchange in plant cells which are sufficiently large and often arranged regularly. Further numerical analysis is required to validate the proposed protocol for more complicated cellular shapes and configurations.

Acknowledgments

DG acknowledges partial support by the Grant ANR-13-JSV5-0006-01 of the French National Research Agency.

Appendix A. Matrix formalism on the interval

In order to compute the PGSE signals, we employ the matrix formalism which was shown to be a rapid, accurate and efficient numerical tool [3,24,95-101]. We illustrate the application of this technique for a particular case of an interval $[-L,L]$ with Neumann boundary condition at the reflecting endpoints, and a semi-permeable barrier at the origin with permeability κ. There are two sets of Laplacian eigenfunctions in this domain:

(i) symmetric eigenfunctions:

$$u_{n,1}(x) = \epsilon_n \cos(\pi n x/L), \qquad \lambda_{n,1} = \pi^2 n^2/L^2, \tag{A.1}$$

enumerated by the index $n = 0,1,2,\ldots$, with $\epsilon_n = 1/\sqrt{L}$ for $n > 0$, and $\epsilon_0 = 1/\sqrt{2L}$. This set includes a constant function $u_{0,1}(x) = (2L)^{-1/2}$.

(ii) antisymmetric eigenfunctions:

$$u_{n,2}(x) = \begin{cases} +\beta_n \cos(\alpha_n(1 - x/L)) & (x > 0), \\ -\beta_n \cos(\alpha_n(1 + x/L)) & (x < 0), \end{cases} \tag{A.2}$$

with $\lambda_{n,2} = \alpha_n^2/L^2$, where α_n $(n = 0,1,2,\ldots)$ satisfy the equation

$$\alpha_n \tan\alpha_n = 2\kappa L/D, \tag{A.3}$$

while the normalization constant β_n is

$$\beta_n = L^{-1/2}\left(1 + \frac{2\kappa L/D}{\alpha_n^2 + 4\kappa^2 L^2/D^2}\right)^{-1/2}. \tag{A.4}$$

Solutions α_n of Eq. (A.3) lie in the intervals $(\pi n, \pi n + \pi/2)$, with $n = 0,1,2,\ldots$.

In what follows, we use the double index (n,j) to distinguish symmetric and antisymmetric eigenfunctions and to enumerate eigenvalues, eigenfunctions, as well as the elements of governing matrices and vectors. We introduce two (infinite-dimensional) matrices $\mathcal{A}$ and $\mathcal{B}$ to represent the Laplace operator and the gradient operator in the Laplacian eigenbasis: $\mathcal{A}_{n,j;n',j'} = \delta_{n,n'}\delta_{j,j'}\lambda_{n,j}$, and

$$\mathcal{B}_{n,j;n',j'} = \int_{-L}^{L} dx u_{n,j}(x) x u_{n',j'}(x). \tag{A.5}$$

The symmetry of eigenfunctions $u_{n,j}$ implies $\mathcal{B}_{n,1;n',1} = \mathcal{B}_{n,2;n',2} = 0$, while

$$\mathcal{B}_{n,1;n',2} = \mathcal{B}_{n',2;n,1} = 2L^2\beta_{n'}\epsilon_n \frac{[(-1)^n - \cos(\alpha_{n'})](\alpha_{n'}^2 + \pi^2 n^2)}{(\alpha_{n'}^2 - \pi^2 n^2)^2}. \tag{A.6}$$

We consider the uniform initial density over the interval $[-R,R]$ (with $R \leqslant L$) in order to reduce the effect of endpoints. The projection of this density onto eigenfunctions is

$$U_{n,j}(R) \equiv \frac{1}{2R}\int_{-R}^{R} dx u_{n,j}(x) = \begin{cases} \epsilon_n \frac{\sin(\pi n R/L)}{\pi n R/L} & (j = 1), \\ 0 & (j = 2). \end{cases} \tag{A.7}$$

Since both endpoints are reflecting, the total number of particles is preserved so that the vector $U(R)$ at $R = L$ has only one nonzero element corresponding to the constant eigenfunction: $U_{n,j}(L) = (2L)^{-1/2}\delta_{n,0}\delta_{j,1}$.

The PGSE signal can be written in the form of a scalar product [3,100]

$$S(g) = \left(U(R)e^{-(D\mathcal{A} - i\gamma g\mathcal{B})\delta}e^{-D\mathcal{A}(\Delta-\delta)}e^{-(D\mathcal{A}+i\gamma g\mathcal{B})\delta}\widetilde{U}\right), \tag{A.8}$$

where $\widetilde{U} = (2L)U(L)$. Since the Laplacian eigenbasis for this problem is known explicitly, the underlying matrix formalism presents a rapid and very accurate numerical tool.

In the matrix formalism for multilayered structures [24], one can choose to distribute the starting points over certain layers. For instance, one can remove the initial magnetization from the first and the last intervals, $[r_0, r_1]$ and $[r_{\ell-1}, r_\ell]$, in order to reduce the effect of reflecting endpoints. If the lengths of these intervals are large as compared to the diffusion length, most nuclei do not reach the reflecting endpoints at r_0 and r_ℓ, thus reducing their effect. For this purpose, Eq. (A.2) from [24] has to be replaced by

$$J_k \equiv \frac{1}{R^d - r_0^d}\int_{r_1}^{r_{\ell-1}} dr r^{d-1} v_{0k}(r) = -\frac{1}{\lambda_{0k}(R^d - r_0^d)}\left[r_{\ell-1}^{d-1}D_{\ell-1}v'_{\ell-1}(r_{\ell-1}) - r_1^{d-1}D_2 v'_2(r_1)\right]. \tag{A.9}$$

References

[1] P.T. Callaghan, Principles of Nuclear Magnetic Resonance Microscopy, Clarendon Press, Oxford, 1991.
[2] W.S. Price, NMR Studies of translational Motion: Principles and Applications, Cambridge University Press, 2009.
[3] D.S. Grebenkov, NMR survey of reflected Brownian motion, Rev. Mod. Phys. 79 (2007) 1077–1137.
[4] D.G. Norris, The effects of microscopic tissue parameters on the diffusion weighted magnetic resonance imaging experiment, NMR Biomed. 14 (2001) 77–93.
[5] D. Le Bihan, Looking into the functional architecture of the brain with diffusion MRI, Nat. Rev. Neuro. 4 (2003) 469–480.
[6] D.S. Tuch, T.G. Reese, M.R. Wiegell, V.J. Wedeen, Diffusion MRI of complex neural architecture, Neuron 40 (2003) 885–895.
[7] J. Frahm, P. Dechent, J. Baudewig, K.D. Merboldt, Advances in functional MRI of the human brain, Prog. Nucl. Magn. Reson. Spectr. 44 (2004) 1–32.
[8] D. Le Bihan, The 'wet mind': water and functional neuroimaging, Phys. Med. Biol. 52 (2007) R57–R90.
[9] D. Le Bihan, H. Johansen-Berg, Diffusion MRI at 25: exploring brain tissue structure and function, NeuroImage 61 (2012) 324–341.
[10] A.S. Verkman, A.N. Van Hoek, T. Ma, A. Frigeri, W.R. Skach, A. Mitra, B.K. Tamarappoo, J. Farinas, Water transport across mammalian cell membranes, Am. J. Physiol. 270 (1996) C12–C30.
[11] J.A. Helpern, R.J. Ordidge, R.A. Knight, The effect of cell membrane water permeabiltiy on the apparent diffusion coefficient of water, in: Proceedings of SMRM, 11th Annual Meeting, Berlin, 1992, p. 1201.
[12] K.R. Brownstein, C.E. Tarr, Importance of classical diffusion in NMR studies of water in biological cells, Phys. Rev. A 19 (1979) 2446–2453.
[13] A.V. Barzykin, K. Hayamizu, W.S. Price, M. Tachiya, Pulsed-field-gradient nmr of diffusive transport through a spherical interface into an external medium containing a relaxation agent, J. Magn. Reson. A 114 (1995) 39–46.

[14] W.S. Price, A.V. Barzykin, K. Hayamizu, M. Tachiya, A model for diffusive transport through a spherical interface probed by pulsed-field gradient NMR, Biophys. J. 74 (1998) 2259–2271.
[15] J.E. Tanner, Transient diffusion in a system partitioned by permeable barriers. Application to NMR measurements with a pulsed field gradient, J. Chem. Phys. 69 (1978) 1748–1754.
[16] F. Crick, Difusion in embryogenesis, Nature 225 (1970) 420–422.
[17] J.E. Tanner, Intracellular diffusion of water, Arch. Biochem. Biophys. 224 (1983) 416–428.
[18] O. Dietrich, A. Hubert, S. Heiland, Imaging cell size and permeability in biological tissue using the diffusion-time dependence of the apparent diffusion coefficient, Phys. Med. Biol. 59 (2014) 3081–3096.
[19] A. Szafer, J. Zhong, J.C. Gore, Theoretical model for water diffusion in tissues, Magn. Reson. Med. 33 (1995) 697–712.
[20] J.C. Ford, D.B. Hackney, Numerical model for calculation of apparent diffusion coefficients (ADC) in permeable cylinders: comparison with measured ADC in spinal cord white matter, Magn. Reson. Med. 37 (1997) 387–394.
[21] E.G. Novikov, D. van Dusschoten, H. van As, Modeling of self-diffusion and relaxation time NMR in multi-compartment systems, J. Magn. Reson. 135 (1998) 522–528.
[22] P.W. Kuchel, C.J. Durrant, Permeability coefficients from NMR q-space data: models with unevenly spaced semi-permeable parallel membranes, J. Magn. Reson. 139 (1999) 258–272.
[23] B.F. Moroney, T. Stait-Gardner, B. Ghadirian, N.N. Yadav, W.S. Price, Numerical analysis of NMR diffusion measurements in the short gradient pulse limit, J. Magn. Reson. 234 (2013) 165–175.
[24] D.S. Grebenkov, Pulsed-gradient spin-echo monitoring of restricted diffusion in multilayered structures, J. Magn. Reson 205 (2010) 181–195.
[25] A.L. Sukstanskii, D.A. Yablonskiy, J.J.H. Ackerman, Effects of permeable boundaries on the diffusion-attenuated MR signal: insights from a one-dimensional model, J. Magn. Reson. 170 (2004) 56–66.
[26] J. Kärger, NMR self-diffusion studies in heterogeneous systems, Adv. Colloid. Interfac. 23 (1985) 129–148.
[27] J. Kärger, H. Pfeifer, W. Heink, Principles and applications of self-diffusion measurements by nuclear magnetic resonance, in: J.S. Waugh (Ed.), Advances in Magnetic Resonance, vol. 12, Academic Press, San Diego, CA, 1988, pp. 1–89.
[28] C.-L. Chin, F.W. Wehrli, S.N. Hwang, M. Takahashi, D.B. Hackney, Biexponential diffusion attenuation in the rat spinal cord: computer simulations based on anatomic images of axonal architecture, Magn. Reson. Med. 47 (2002) 455–460.
[29] T. Niendorf, R.M. Dijkhuizen, D.G. Norris, M. van Lookeren Campagne, K. Nicolay, Biexponential diffusion attenuation in various states of brain tissue: implications for diffusion-weighted imaging, Magn. Reson. Med. 36 (1996) 847–857.
[30] R.V. Mulkern, H. Gudbjartsson, C.F. Westin, H.P. Zengingonul, W. Gartner, C.R. Guttmann, R.L. Robertson, W. Kyriakos, R. Schwartz, D. Holtzman, F.A. Jolesz, S.E. Maier, Multicomponent apparent diffusion coefficients in human brain, NMR Biomed. 12 (1999) 51–62.
[31] C.A. Clark, D. Le Bihan, Water diffusion compartmentation and anisotropy at high b values in the human brain, Magn. Reson. Med. 44 (2000) 852–859.
[32] A. Schwarcz, P. Bogner, P. Meric, J. Correze, Z. Berente, J. Pal, F. Gallyas, T. Doczi, B. Gillet, J. Beloeil, The existence of biexponential signal decay in magnetic resonance diffusion-weighted imaging appears to be independent of compartmentalization, Magn. Reson. Med. 51 (2004) 278–285.
[33] Z. Ababneh, H. Beloeil, C.B. Berde, G. Gambarota, S.E. Maier, R.V. Mulkern, Biexponential parameterization of diffusion and T2 relaxation decay curves in a rat muscle edema model: decay curve components and water compartments, Magn. Reson. Med. 54 (2005) 524–531.
[34] J.H. Lee, C.S. Springer, Effects of equilibrium exchange on diffusion-weighted NMR signals: the diffusigraphic shutter-speed, Magn. Reson. Med. 49 (2003) 450–458.
[35] G.J. Stanisz, Diffusion MR in biological systems: tissue compartments and exchange, Isr. J. Chem. 43 (2003) 33–44.
[36] D.S. Grebenkov, Use, misuse, and abuse of apparent diffusion coefficients, Conc. Magn. Reson. 36A (2010) 24–35.
[37] E. Fieremans, D.S. Novikov, J.H. Jensen, J.A. Helpern, Monte Carlo study of a two-compartment exchange model of diffusion, NMR Biomed. 23 (2010) 711–724.
[38] J. Coatleven, H. Haddard, J.-R. Li, A new macroscopic model including membrane exchange for diffusion MRI, SIAM J. Appl. Math. 74 (2014) 516–546.
[39] G.J. Stanisz, A. Szafer, G.A. Wright, R.M. Henkelman, An analytical model of restricted diffusion in bovine optic nerve, Magn. Reson. Med. 37 (1997) 103–111.
[40] C. Meier, W. Dreher, D. Leibfritz, Diffusion in compartmental systems. I. A comparison of an analytical model with simulations, Magn. Reson. Med. 50 (2003) 500–509.
[41] C. Meier, W. Dreher, D. Leibfritz, Diffusion in compartmental systems. II. Diffusion-weighted measurements of rat brain tissue in vivo and postmortem at very large b-values, Magn. Reson. Med. 50 (2003) 510–514.
[42] J. Andrasko, Water diffusion permeability of human erythrocytes studied by a pulsed gradient NMR technique, Biochim. Biophys. Acta 428 (1976) 304–311.
[43] M.D. Herbst, J.H. Goldstein, A review of water diffusion measurement by NMR in human red blood cells, Am. J. Physiol. Cell. Physiol. 256 (1989) C1097–C1104.
[44] A.R. Waldeck, P.W. Kuchel, A.J. Lennon, B.E. Chapman, NMR diffusion measurements to characterise membrane transport and solute binding, Prog. Nucl. Mag. Res. Spectr. 30 (1997) 39–68.
[45] G.J. Stanisz, J.G. Li, G.A. Wright, R.M. Henkelman, Water dynamics in human blood via combined measurements of T2 relaxation and diffusion in the presence of gadolinium, Magn. Reson. Med. 39 (1998) 223–233.
[46] Y. Roth, A. Ocherashvilli, D. Daniels, J. Ruizcabello, S. Maier, A. Orenstein, Y. Mardor, Quantification of water compartmentation in cell suspensions by diffusion-weighted and T2-weighted MRI, Magn. Reson. Imaging 26 (2008) 88–102.
[47] I. Åslund, A. Nowacka, M. Nilsson, D. Topgaard, Filter-exchange PGSE NMR determination of cell membrane permeability, J. Magn. Reson. 200 (2009) 291–295.
[48] J. Pfeuffer, W. Dreher, E. Sykova, D. Leibfritz, Water signal attenuation in diffusion-weighted H NMR experiments during cerebral ischemia: influence of intracellular restrictions, extracellular tortuosity, and exchange, Magn. Reson. Imaging 16 (1998) 1023–1032.
[49] J.D. Quirk, G.L. Bretthorst, T.Q. Duong, A.Z. Snyder, C.S. Springer, J.J.H. Ackerman, J.J. Neil, Equilibrium water exchange between the intra- and extracellular spaces of mammalian brain, Magn. Reson. Med. 50 (2003) 493–499.
[50] M. Nilsson, J. Lätt, E. Nordh, R. Wirestam, F. Strahlberg, S. Brockstedt, On the effects of a varied diffusion time in vivo: is the diffusion in white matter restricted?, Magn Reson. Imaging 27 (2009) 176–187.
[51] H.M. McConnell, Reaction rates by nuclear magnetic resonance, J. Chem. Phys. 28 (1958) 430–431.
[52] T. Conlon, R. Outhred, Water diffusion permeability of erythrocytes using an NMR technique, Biochim. Biophys. Acta 288 (1972) 354–361.
[53] M.C. Steward, M.J. Garson, Water permeability of Necturus gallbladder epithelial cell membranes measured by nuclear magnetic resonance, J. Membr. Biol. 86 (1985) 203–210.
[54] J.E.M. Snaar, H. Van As, Probing water compartments and membrane permeability in plant cells by 1H NMR relaxation measurements, Biophys. J. 63 (1992) 1654–1658.
[55] C.S. Landis, X. Li, F.W. Telang, P.E. Molina, I. Palyka, G. Vetek, C.S. Springer, Equilibrium transcytolemmal water-exchange kinetics in skeletal muscle in vivo, Magn. Reson. Med. 42 (1999) 467–478.
[56] R.A. Brooks, F. Moiny, P. Gillis, T2-shortening by weakly magnetized particles: the chemical exchange model, Magn. Reson. Med. 45 (2001) 1014–1020.
[57] P.P. Mitra, P.N. Sen, L.M. Schwartz, P. Le Doussal, Diffusion propagator as a probe of the structure of porous media, Phys. Rev. Lett. 68 (1992) 3555–3558.
[58] P.P. Mitra, P.N. Sen, Effects of microgeometry and surface relaxation on NMR pulsed-field-gradient experiments: simple pore geometries, Phys. Rev. B 45 (1992) 143–156.
[59] P.P. Mitra, P.N. Sen, L.M. Schwartz, Short-time behavior of the diffusion coefficient as a geometrical probe of porous media, Phys. Rev. B 47 (1993) 8565–8574.
[60] L.L. Latour, P.P. Mitra, R.L. Kleinberg, C.H. Sotak, Time-dependent diffusion coefficient of fluids in porous media as a probe of surface-to-volume ratio, J. Magn. Reson. A 101 (1993) 342–346.
[61] M.D. Hürlimann, K.G. Helmer, L.L. Latour, C.H. Sotak, Restricted diffusion in sedimentary rocks. determination of surface-area-to-volume ratio and surface relaxivity, J. Magn. Reson. A 111 (1994) 169–178.
[62] L.L. Latour, K. Svoboda, P.P. Mitra, C.H. Sotak, Time-dependent diffusion of water in a biological model system, Proc. Natl. Acad. Sci. USA 91 (1994) 1229–1233.
[63] D.S. Novikov, E. Fieremans, J.H. Jensen, J.A. Helpern, Random walks with barriers, Nat. Phys. 7 (2011) 508–514.
[64] D.S. Novikov, J.H. Jensen, J.A. Helpern, E. Fieremans, Revealing mesoscopic structural universality with diffusion, Proc. Nat. Ac. Sci. 111 (2014) 5088–5093.
[65] J.G. Powles, M.J.D. Mallett, G. Rickayzen, W.A.B. Evans, Exact analytic solutions for diffusion impeded by an infinite array of partially permeable barriers, Proc. R. Soc. London, Ser. A: Math. Phys. Sci. 436 (1992) 391–403.
[66] S.N. Hwang, C.L. Chin, F.W. Wehrli, D.B. Hackney, An image-based finite difference model for simulating restricted diffusion, Magn. Reson. Med. 50 (2003) 373–382.
[67] J. Xu, M.D. Does, J.C. Gore, Numerical study of water diffusion in biological tissues using an improved finite difference method, Phys. Med. Biol. 52 (2007) N111–N126.
[68] D.V. Nguyen, J.-R. Li, D.S. Grebenkov, D. Le Bihan, An efficient finite-elements code to simulate diffusion MRI signals in complex tissue geometries, J. Comput. Phys. 263 (2014) 283–302.
[69] K.M. Donahue, R.M. Weisskoff, D. Burstein, Water diffusion and exchange as they influence contrast enhancement, J. Magn. Reson. Imag. 7 (1997) 102–110.
[70] C.R. House, Water Transport in Cells and Tissues, Edward Arnold, Ltd., London, UK, 1974. p. 156.
[71] A. Finkelstein, Water Movement Through Lipid Bilayers, Pores, and Plasma Membranes: Theory and Reality, John Wiley & Sons, New York, 1987. p. 155.
[72] C. Labadie, J.-H. Lee, G. Vetek, C.S. Springer, Relaxographic imaging, J. Magn. Reson. B 105 (1994) 99–112.
[73] J.V. Sehy, A.A. Banks, J.J.H. Ackerman, J.J. Neil, Importance of intracellular water apparent diffusion to the measurement of membrane permeability, Biophys. J. 83 (2002) 2856–2863.

[74] T.H. Haines, L.S. Liebovitch, A molecular mechanism for the transport of water across phospholipid bilayers, in: E.A. Disalvo, S.A. Simon (Eds.), Permeability and Stability of Lipid Bilyaers, CRC Press, 1995, pp. 123–136.
[75] S.A. Gradilone, J.E. Ochoa, F. Garcia, M.C. Larocca, J.M. Pellegrino, R.A. Marinelli, Hepatocyte membrane water permeability measured by silicone layer filtering centrifugation, Anal. Biochem. 302 (2002) 104–107.
[76] D.G. Stout, P.L. Steponkus, L.D. Bustard, R.M. Cotts, Water permeability of chlorella cell membranes by nuclear magnetic resonance: measured diffusion coefficients and relaxation times, Plant Physiol. 62 (1978) 146–151.
[77] M.C. Steward, Y. Seo, J.M. Rawlings, R.M. Case, Water permeability of acinar cell membranes in the isolated perfused rabbit mandibular salivary gland, J. Physiol. 431 (1990) 571–583.
[78] T. Imae, H. Shinohara, M. Sekino, S. Ueno, H. Ohsaki, K. Mima, K. Ootomo, Estimation of cell membrane permeability of the rat brain using diffusion magnetic resonance imaging, J. Appl. Phys. 103 (2008) 07A311.
[79] R.A. Garrick, F.P. Chinard, Membrane permeability of isolated lung cells to nonelectrolytes at different temperatures, Am. J. Physiol. 243 (1982) C285–C292.
[80] D.A.T. Dick, The permeability coefficient of water in the cell membrane and the diffusion coefficient in the cell interior, J. Theor. Biol. 7 (1964) 504–531.
[81] H. Van As, Intact plant MRI for the study of cell water relations, membrane permeability, cell-to-cell and long-distance water transport, J. Exper. Botany 58 (2007) 743–756.
[82] D.S. Grebenkov, Exploring diffusion across permeable barriers at high gradients. II. Localization regime, J. Magn. Reson 248 (2014) 164–176.
[83] D.S. Grebenkov, B.-T. Nguyen, Geometrical structure of Laplacian eigenfunctions, SIAM Rev. 55 (2013) 601–667.
[84] E.O. Stejskal, Use of spin echoes in a pulsed magnetic-field gradient to study anisotropic, restricted diffusion and flow, J. Chem. Phys. 43 (1965) 3597–3603.
[85] J.E. Tanner, E.O. Stejskal, Restricted self-diffusion of protons in colloidal systems by the pulsed-gradient, spin-echo method, J. Chem. Phys. 49 (1968) 1768–1777.
[86] P.T. Callaghan, A. Coy, D. MacGowan, K.J. Packer, F.O. Zelaya, Diffraction-like effects in NMR diffusion studies of fluids in porous solids, Nature 351 (1991) 467–469.
[87] B. Balinov, B. Jönsson, P. Linse, O. Söderman, The NMR self-diffusion method applied to restricted diffusion. Simulation of echo attenuation from molecules in spheres and between planes, J. Magn. Reson. A 104 (1993) 17–25.
[88] A. Coy, P.T. Callaghan, Pulsed gradient spin echo nuclear magnetic resonance for molecules diffusing between partially reflecting rectangular barriers, J. Chem. Phys. 101 (1994) 4599–4609.
[89] M.H. Blees, The effect of finite duration of gradient pulses on the pulsed-field-gradient NMR method for studying restricted diffusion, J. Magn. Reson. A 109 (1994) 203–209.
[90] P. Linse, O. Söderman, The validity of the short-gradient-pulse approximation in NMR studies of restricted diffusion. Simulations of molecules diffusing between planes, in cylinders and spheres, J. Magn. Reson. A 116 (1995) 77–86.
[91] L.Z. Wang, A. Caprihan, E. Fukushima, The narrow-pulse criterion for pulsed-gradient spin-echo diffusion measurements, J. Magn. Res. Series A. 117 (1995) 209–219.
[92] P.T. Callaghan, Pulsed gradient spin echo nmr for planar, cylindrical and spherical pores under conditions of wall relaxation, J. Magn. Reson. A 113 (1995) 53–59.
[93] A.F. Frhlich, L. Stergaard, V.G. Kiselev, Effect of impermeable boundaries on diffusion-attenuated MR signal, J. Magn. Reson. 179 (2006) 223–233.
[94] A.L. Sukstanskii, J.J.H. Ackerman, D.A. Yablonskiy, Effects of barrier-induced nuclear spin magnetization inhomogeneities on diffusion-attenuated MR signal, Magn. Reson. Med. 50 (2003) 735–742.
[95] A. Caprihan, L.Z. Wang, E. Fukushima, A multiple-narrow-pulse approximation for restricted diffusion in a time-varying field gradient, J. Magn. Reson. A 118 (1996) 94–102.
[96] P.T. Callaghan, A simple matrix formalism for spin echo analysis of restricted diffusion under generalized gradient waveforms, J. Magn. Reson. 129 (1997) 74–84.
[97] A.V. Barzykin, Exact solution of the Torrey–Bloch equation for a spin echo in restricted geometries, Phys. Rev. B 58 (1998) 14171–14174.
[98] A.V. Barzykin, Theory of spin echo in restricted geometries under a step-wise gradient pulse sequence, J. Magn. Reson. 139 (1999) 342–353.
[99] S. Axelrod, P.N. Sen, Nuclear magnetic resonance spin echoes for restricted diffusion in an inhomogeneous field: methods and asymptotic regimes, J. Chem. Phys. 114 (2001) 6878–6895.
[100] D.S. Grebenkov, Laplacian eigenfunctions in NMR I. A numerical tool, Conc. Magn. Reson. 32A (2008) 277–301.
[101] D.S. Grebenkov, Laplacian eigenfunctions in NMR. II. Theoretical advances, Conc. Magn. Reson. 34A (2009) 264–296.